A. BBSO Update

On Sept 14, 2015, our current three-year AFOSR FA9550-15-1-0322 grant (Goode, PI) started, which has supported Vasyl Yurchyshyn who performs data collection, processing, analysis, and interpretation yielding new scientific results. Our success is built on prior AFOSR support for the Goode Solar Telescope (GST, formerly New Solar Telescope), and its instrumentation.

GST is the first facility class solar telescope built in the U.S. in a generation. Under current AFOSR support, the GST was used to observe the photosphere, chromosphere and up to the transition region with unprecedented resolution to elucidate the fundamental nature of the dynamics of solar magnetism and its evolution. As always, we use the GST in sustained campaigns with other observatories supporting the community's efforts to determine the origin of "space weather", which arises from solar magnetic storms and can have deleterious effects on satellites, as well as the terrestrial power grid, telecommunications, and other aspects of human civilization. These partners include ALMA (Atacama Large Millimeter/submillimeter Array), 1.5-m GREGOR Solar Telescope, 1-m NVST (New Vacuum Solar Telescope, China), NSO's DST (Dunn Solar Telescope), McP (McMath-Pierce Solar Telescope), SOLIS (Synoptic Optical Long-term Investigation of the Sun), as well as NASA's Hi-C II, IRIS (Interface Region Imaging Spectrograph), and *Hinode* Missions. Joint observations account for 60 - 80% of the GST observing time annually.

The GST is the pathfinder for the Daniel K. Inouye Solar Telescope (DKIST) currently built in Hawaii and it will operate adjacent to the Air Force AEOS telescope atop Haleakala, Maui. Both the GST and the 4 m DKIST have off-axis designs. The GST will dominate U.S. ground-based observations at least until early in the coming decade. After the DKIST is online, the GST will still have an essential role. Currently the DKIST team is organizing a series of workshops to devise observing plans for early DKIST operation in which we actively participate. It is expected that the DKIST will be over-subscribed and some of the submitted Science Use Cases that do not require 4-m aperture will be recommended to seek observing time with other telescopes with the GST being a likely candidate. With the closure of NSO mid-aperture solar telescopes, the shortage of telescope time may be even more palpable since there is an uptick in community interest toward high-resolution observations driven by the DKIST nearing completion.

We will continue to make systematic, fundamental changes in the observatory's instrumentation to ensure a unique and significant scientific role for BBSO. The resulting improvements in data quality helped our research group advance our understanding of the Sun, as evidenced by the list of the publications supported, in part, by AFOSR funding.

BBSO highly prizes its special role in the education of the next generation of scientists who build instruments. As a university-based astrophysics facility, the GST provides a unique opportunity for both postdoctoral and graduate student involvement, directly impacting their education and training, and contributes to the revitalization and growth of the solar physics community.

BBSO is part of NJIT's Center for Solar-Terrestrial Research (CSTR) that has an unpaid, outside Advisory Board that meets bi-annually to critique NJIT's comprehensive solar-terrestrial program. The Board's report is made to the upper management of NJIT, which respects their advice and uses it to improve BBSO and the other facilities NJIT operates (in Antarctica, Peru and California).

Since NJIT began operating BBSO, its telescope time and data have been open to the community. Many outside scientists have had observing time and students from around the world are using BBSO data as a central part of their thesis work. Data requests come to BBSO on a daily basis and we have an automatic data distribution system in place. We only ask that users of GST data acknowledge BBSO and its support by federal agencies in their resulting publications. BBSO achievements in instrumentation are briefly listed in Section B.1, while for the remainder of this section, we focus on the highlights of some of our scientific and instrument achievements under current AFOSR support.

Key among what we propose are: (1) large-scale phenomena like flares and sunspots will be studied with the GST providing high cadence, sub-second photometric measurements and 15 s cadence vector magnetograms, which will enable us to address fundamental problems of energy storage and the initiation of eruptions from active regions, which is critical for predicting the onset and intensity of dynamic solar activity events and the resulting level of space radiation; (2) heating of active region loops will be addressed by taking a closer look at the loop foot-points. This will be the first study of this kind utilizing high resolution GST/NIRIS observations; (3) small-scale spatial structure, oscillations and waves in a sunspot. We propose to further explore these events and determine their connection to the heating of coronal loops above sunspots, as seen by SDO and IRIS data. (4) the rapidly increasing volume of GST data presents a challenge for archiving and community access and requires a new approach to data storage, tagging and distribution. We will develop a pipeline that will enable us to automatically extract information from the images (e.g., object: sunspot, pores, quiet sun, filament; event: dynamic fibrils and jets, flares, flux emergence), store these meta-data and provide them to scientific knowledge-based catalogs.

A.1 Principal MCAO Progress: Clear Widens the Field for Observations of the Sun

The stunning successes of solar adaptive optics (AO) have come from systems with a single deformable mirror (DM) in which only the isoplanatic patch (typically $\leq 10''$ in visible light under good seeing conditions) can be corrected to the diffraction limit with decreasing correction as distance from the patch increases. Multi-conjugate AO (MCAO) setup has two, or more, DMs to correct anisoplanatism with each DM being conjugated to a different layer of atmospheric turbulence. MCAO is a demonstrated technique for correcting atmospheric turbulence over a wide field of view (FOV) for observations of the night sky (Marchetti et al., 2003; Rigaut et al., 2014; Neichel et al., 2014b), and the Gemini South MCAO system (GeMS) is the nighttime system routinely used for astronomical observations (e. g. Neichel et al., 2014a). Wavefront sensing in nighttime MCAO is difficult because multiple laser guide stars (LGSs) are needed for tomographic wavefront reconstruction. The GeMS uses five LGSs and three natural guide stars,

BBSO *Clear* (Schmidt et al., 2017) is the first solar MCAO system to significantly improve (triple) the corrected FOV. The Sun is a natural target for extended object wavefront sensing; any number of "target stars" can be made from the 2-D structure of the Sun by using correlations from Shack-Hartmann wavefront sensing, which is the technique being used in our approach to solar AO. This is technically difficult, but wide-field, diffraction-limited correction is the holy grail for addressing the fundamental dynamics of our star, and must be done. We have enjoyed noteworthy successes. Our motivation to build such a challenging system comes from the fact that the GST is the only solar telescope in the U.S. having sufficient aperture and modulation transfer function to resolve what is generally regarded as the fundamental scale of the Sun's surface. This will remain true until the advent of the 4 m aperture DKIST that is due for first light in 2020, even then only the GST can be devoted to extended space weather studies.

It is important to bear in mind that magnetic field dynamics are the cause of the Sun's powerful, explosive and non-local events, like flaring and coronal mass ejections (CMEs), which can cover upwards of $\sim 50''$ and occasionally more. Spectro-polarimetric measurements of magnetic fields require imaging that is temporally stable over the entire FOV. The vast majority of solar observing programs would tremendously benefit from diffraction limited resolution over an extended FOV. For example, a single supergranular cell (convective flow pattern that reflects the organization of the magnetic network of the Sun) is $\sim 30''$ in diameter. To study magnetic reconnection events in the network boundaries, it would be invaluable to have diffraction limited resolution over a FOV that covers two network cells. Further, a typical sunspot (see Fig. 2) may cover $\sim 50''$, which is about two-thirds the GST FOV. Sunspot evolution, flares and CMEs are quite non-local phenomena, with nearly simultaneous interconnected dynamics often

spread over the entire FOV. If a flare were to be registered in the FOV it is likely that it would not entirely occur within the isoplanatic patch. We have ~~studies~~ several such events and every time important details of flare evolution were ~~omitted~~ due to inferior resolution outside the isoplanatic patch (see references below). Typically, image reconstruction, such as speckle, is used to correct the full field to the diffraction limit at the cost of temporal resolution being reduced by a factor of ~100, which yields time steps of a few seconds at best, rather than the subsecond resolution (for a review see Nordlund et al. (2009)) required to probe the fundamentals of magnetic field dynamics. Meaningful image reconstruction relies on an unchanging FOV during each burst so the reconstruction itself is problematic during the most scientifically significant moments of large eruptive flares that are at the origin of large "space-weather" events (for details see http://swpc.noaa.gov), which can impact the terrestrial environment including satellites.

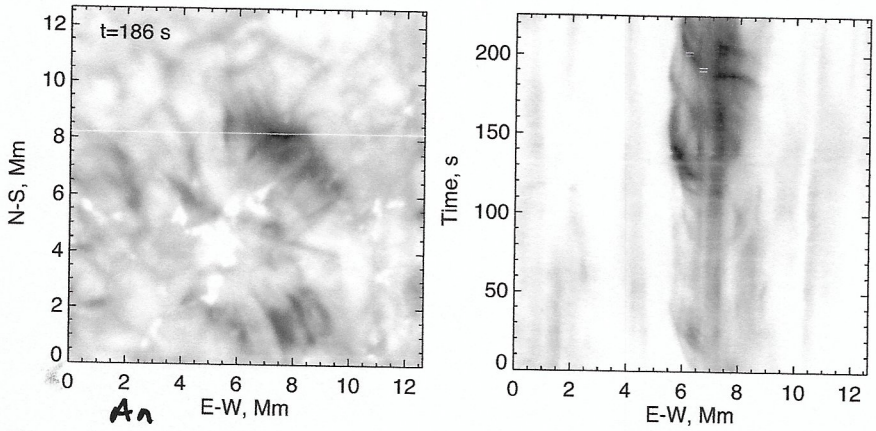

Figure 1: *A Hα-1.0Å GST Clear image obtained on 28 Sept 2017 (left) and the corresponding space-time (x-t) plot (right) made along the horizontal line in the left panel. The left slanted dark tracks in the right panel at $x = 6-8$ Mm that begin at $t = 120$ s reveal that the jet-like features under the horizontal line were translationally moving to the left at the rate of about 100 km/s. During a 10 s interval the jets are displaced by about 1 Mm, which exceed their cross-section (< 0.5 Mm). The two sets of short line segments at $t = 190$ s and $t = 200$ s indicate the positions of the jet we would have registered if the observations were to proceed at a typical 10 s cadence. In this case the large jet displacement (1 Mm) would made it impossible ~~neither accurately~~ track the event ~~not accurate event interpretation (two events? high frequency oscillations?)~~.*

The above arguments are further demonstrated in Fig. 1, which shows an Hα-1.0Å *Clear* snapshot of a quiet Sun area (left) and an x-t plot (right) made along an image row indicated by the horizontal line in the left panel. The dark jet-like features under the horizontal line were shifting to the left at the rate of ~ 100 km/s, which is evident from the left slanted tracks that start at $t = 120$ s in the $x = 6-8$ Mm range. During a 10 s interval the jets were displaced by about 0.8 Mm, which exceeds their cross-section (< 0.25 Mm). The two short vertical lines in the right panel at $x = 6.5$ Mm and $y = 190$ s indicate positions of the jet that we would registered were we to observe the same event with 10 s cadence, which is typical cadence for chromospheric observations. In this case the shift is to large to even reliably identify it as one event, so we would interpret it as two separate jets or high frequency oscillations. The MCAO Hα data cadence was 0.25 s and the x-t plot accurately captured all rapid jet displacements. Accurate knowledge of such small-scale active phenomena is crucial for untangling such solar physics problems as flare initiation and coronal heating.

Implementing operational solar MCAO has been an essential, but challenging task. Owing to its proximity, various solar structures of various scales (such as granulation, pores, and sunspots, see Fig. 2), offer innumerable "guide regions" (solar equivalent of guide stars) and enough information to reconstruct the optical turbulence in Earth's atmosphere even though it is a single star. In the current *Clear* setup we use nine guide regions (divide the FOV into nine regions and take whatever is present in each region to guide the reconstruction) and the three DMs are conjugated to i) the pupil with a depth of field (DoF)

of ∼1 km, ii) an approximately 2 km DoF for the DM conjugated to 3 km, and iii) a DoF of about 3 km for the DM conjugated to 8 km to *continuously cover heights from 0 to 11 km with the reduced FOV for wavefront sensing*.

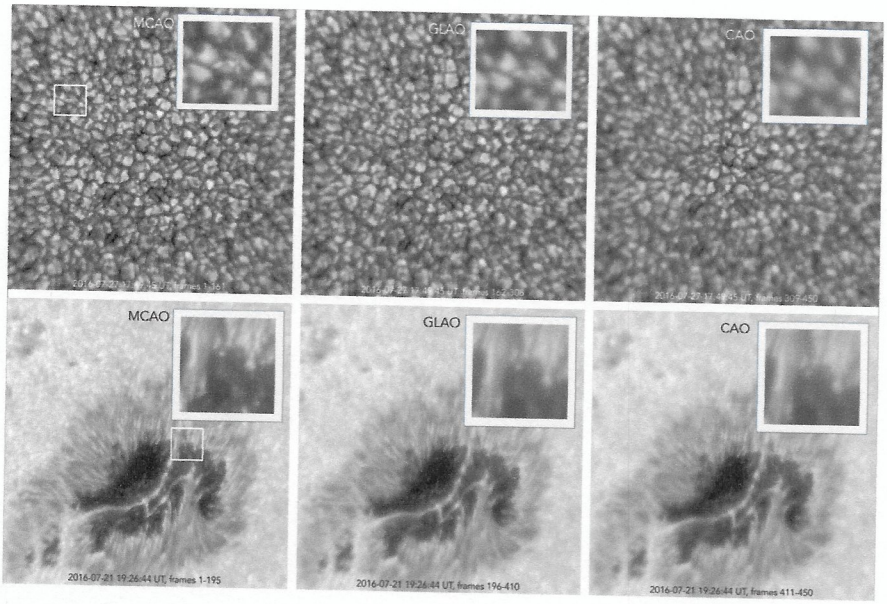

Figure 2: *TiO filter (705.7 nm) 53″ × 53″ images taken with MCAO, GLAO, and CAO correction using the GST Clear on 2016 July 27 at 17:45:48 UT (top row) and 2016 July 21 at 19:26:44 UT (bottom). Exposure time was 1.6 ms for the granulation bursts and 11 ms for the sunspot. The white boxes in the left images indicate the FOV and positions of the corresponding insets. Real-time movies are available online at https:/cuna.nso.edu/clear-preview.*

Results from the *first ever clearly and easily visible successful solar MCAO imaging system* are shown in Fig. 2 (Schmidt et al., 2017). During this first truly successful experiment performed in July 2016, we recorded data using a titanium oxide line (TiO 705.7 ± 5 nm) interference filter. We took numerous short exposure bursts of 450 frames operating at 14.7 frames per second resulting in a total time span of approximately 31 s. Each burst contained about 150 frames (10 sec) with continuous MCAO, ground layer AO (GLAO), and single DM classical AO (CAO) correction. Each panel in Fig. 2 is a superposition of 150 MCAO, GLAO, and CAO frames used without any post-processing of the images.

The control software, KAOS Evo 2 originally developed by Berkefeld et al. (2012) for the GREGOR telescope, enabled us to switch the mode of AO correction instantaneously without losing lock. These bursts are short enough to be interpreted as *quasi-simultaneous* observations with CAO, GLAO, and MCAO correction. In order to rule out that the perceived AO effects are due to unnoticeable seeing changes that may have happened when we toggled the AO mode, we recorded numerous such bursts. In the CAO mode, we used the pupil DM and the central guide-region only, the other DMs were at rest and off-axis guide-regions were ignored. In GLAO mode, we equally considered all nine guide-regions to control the pupil DM, while the higher DMs were still at rest. From simultaneously recorded control loop telemetry data, we can identify the frames in each burst that were corrected in MCAO, GLAO, or CAO manner, respectively.

In the upper left panel of Fig. 2, the great improvement is obvious with $< 0''.2$ intergranular lane bright points (Goode et al., 2010) being easily apparent (see insets) even at the edge of the $\sim 35''$ corrected FOV — the setup that was aimed for a $35''$ corrected FOV and achieved it. In the lower left panel, the fibril structure of the umbra and penumbra look clear, as is the granular field compared to GLAO and CAO results (compare insets). Images like those in Fig. 2 were seen many times during the ten day observing run near the end of July 2016 and three runs in Summer of 2017. Another way to understand Fig. 2 is to examine the generalized Fried parameter (Cagigal & Canales, 2000), which measures Fried parameter across the field. It can be computed using the KISIP image reconstruction

software (Wöger et al., 2008). Inspection of Figs. 2 and 3 reveals the improvement that the MCAO system contributed: the generalized Fried parameter is maximal for the upper left image indicating that nearly the entire FOV is at the diffraction limit. It is noteworthy that this was achieved on a granular field, which makes the MCAO performance even more impressive because it is harder to lock and keep *any* AO system locked on the relatively low-contrast granulation compared to the rather high-contrast features like pores. The rightmost panels of Fig. 2 show superposed images gained with CAO correction. Relatively small isoplanatic patches are apparent near the center of the FOV. One can see advantages for using either CAO or GLAO depending on the requirements of the observations with CAO providing better image detail in a small FOV, while the single DM GLAO performance resulted in a lower but more homogeneous image detail over the field compared to CAO correction. We will use GLAO and CAO from the outset of the work proposed here.

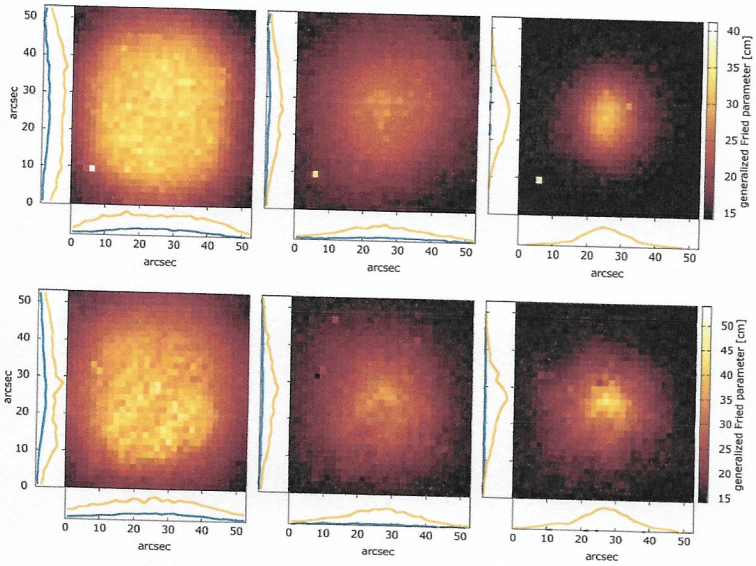

Figure 3: *Generalized Fried parameter (Cagigal & Canales, 2000) across the field of view in the images shown in Fig. 2. The yellow lines along the ordinate and abscissa represent the relative intensities down and across the middle of the field, whereas the blue lines represent the corresponding relative intensities along the margins. For both rows, the full-width at half-maximum in the CAO yellow is* $\sim 10''$*, while that for the MCAO is* $\sim 30''$*.*

Even though we have had runs in which lock has been held for nearly two hours and we have obtained impressive images with MCAO, we are still in an experimental stage. GLAO *is* in regular operation, but MCAO will not be a regular instrument until the second year of the proposed work. We are working now on a system that will feed the MCAO corrected light into existing instrumentation such as the narrow-band Visible Image Spectrometer (VIS) and Near InfraRed Imaging Spectro-polarimeter (NIRIS). The instrumental and software works are underway at this writing, so we conservatively hold back promising use of MCAO in the first year of the work proposed here.

A.2 Principal Science Results from Current AFOSR Support

Fine Structure of White Light Emission. For a long time white light (WL) emission was thought to be associated only with the strongest X-ray flares since it was believed that only these are capable of depositing the necessary amount of energy deep enough in the solar atmosphere to increase the intensity of the Balmer and Paschen continua. As the temporal and spatial resolution of solar instrumentation has improved, the "big flare" syndrome was questioned by detection of WL emission in weak C-class flares. Using high resolution data from GST we studied the fine spatial and temporal structure of an M1.3 WL flare observed near the west solar limb. The strong and compact WL cores were measured to be ~ 0.15 Mm across with an area of about 10^{14}cm^2. This is so far the highest resolution observations of a WL flare. The observed TiO enhancements are not normally distributed and are structured by the magnetic field of the penumbra. Several of the TiO cores were not co-spatial with the Hα emission, which suggests that the TiO and chromospheric emission did not originate in the same chromospheric volume, as some models suggest. We thus conclude that fine temporal and spatial structure of the WL flare was largely defined by the associated magnetic fields, which favors the direct heating models, where

the flare energy is directly deposited in the temperature minimum region by the accelerated electrons.

Study of an Eruptve Flare Triggered by Flux Emergence. Using multiwavelength observations, we studied a slow-rise, multistep X1.6 flare that began on 7 November 2014 as a localized eruption of core fields inside a δ-sunspot and later engulfed the entire active region. This flare was accompanied by a fast and wide coronal mass ejection and two systems of post-eruption arcades and several J-shaped flare ribbons formed during the flare showing extremely fine details and irreversible changes in the photospheric magnetic fields. The ground-based GST data along with HMI magnetic field measurements present evidence that the flare and the eruption were directly triggered by a flux emergence that occurred inside a δ-sunspot at the boundary between two umbrae. This event also represents an example of the formation of an unstable flux rope that led the eruption.

Flux Rope Formation by Series of Magnetic Reconnections in the Chromosphere. Using high-resolution GST data we report direct evidence of merging and reconnection of cool Hα loops in the chromosphere during two homologous B and C class flares caused by a shearing motion at the footpoints of two loops. The reconnection between these loops caused the formation of an unstable flux rope that showed counter-clockwise rotation. The flux rope could not reach the height of torus instability and failed to fully erupt. HMI magnetograms revealed rotation of the negative and positive polarity sunspots in the opposite directions. Rapid photospheric flux cancellation (duration 20-30 min, rate $\approx 3.44 \times 10^{20}$ Mx/h) was observed during the event. To the best of our knowledge, such a clear interaction of chromospheric loops along with rapid flux cancellation has not been reported before.

Modeling a Confined Flare in Super Solar AR 12192. We studied the physical mechanism of a major X-class solar flare that occurred in the super NOAA AR 12192 using data-driven numerical MHD modeling complemented with observations. With the evolving magnetic fields observed at the solar surface as the bottom boundary input, we drive an MHD system to evolve self-consistently in correspondence with the realistic coronal evolution. During a two-day time interval, the modeled coronal field was slowly stressed by the photospheric field evolution, which gradually created a large-scale coronal current sheet, i.e., a narrow layer with intense current, in the core of the AR. The current layer was successively enhanced until it became so thin that a tether-cutting reconnection between the sheared magnetic arcades set in, which led to a flare. The modeled reconnecting field lines and their footpoints match well the observed hot flaring loops and the flare ribbons, respectively, suggesting that the model has successfully "reproduced" the macroscopic magnetic process of the flare. In particular, with these simulations, we explained why this event is a confined eruption. It is the consequence of the reconnection in a shared arcade instead of a newly formed flux rope. We also found a much weaker magnetic implosion effect compared to many other X-class flares.

List of Publications supported by AFOSR FA9550-15-1-0322 Grant

1. *Clear Widens the Field for Observations of the Sun with Multi-conjugate Adaptive Optics*, 2017, Schmidt, D., Gorceis, N., Goode, P.R., et al., 2017, A&A, 597, L8
2. *High Resolution Observations of a White Light Flare with NST*, 2017, Yurchyshyn, V., Kumar, P., Abramenko, V., Xu, Y., Goode, P., Cho, K.-S., & Lim, E.K., Astroph. J., 838/1, article.id 32
3. *Chromospheric Plasma Ejections in a Light Bridge of a Sunspot*, 2017, Song, D., Chae, J., Yurchyshyn, V., et al., Astrophys. J. 835/2, article id. 240, 10 pp
4. *Pre-eruption Oscillations in Thin and Long Features in a Quiescent Filament*, 2016, Joshi, A. D.; Hanaoka, Y., Suematsu, Y., et al., Astrophys. J. 833/2, article id. 243, 9 pp
5. *Multi-wavelength Study of Transition Region Penumbral Subarcsecond Bright Dots Using IRIS and NST*, 2016, Deng, N., Yurchyshyn, V., Tian, H., Astrophys. J., 829/2, article id. 103, 8 pp
6. *Fine-scale Photospheric Connections of Ellerman Bombs*, 2016, Yang, H., Chae, J., Lim, E., et al., Astrophys. J., 829/2, article id. 100, 11 pp
7. *Observations of a Series of Flares and Associated Jet-like Eruptions Driven by the Emergence of Twisted Magnetic Fields*, 2016, Lim, E.K., Yurchyshyn, V., Park, S.-H., et al., Astrophys. J., 817/1, article.id 39
8. *Multiwavelength Observations of a Slow-rise, Multistep X1.6 Flare and the Associated Eruption*, 2015,

Yurchyshyn, V., Kumar, P., Cho, K.-S., et al., Astrophys. J., 812/2, article.id 172
9. Simultaneous observation of a hot explosion by NST and IRIS, 2015, Kim, Y.-H., Yurchyshyn, V., Bong, S-C., et al., Astrophys. J., 810/1, article.id 38
10. Formation and Eruption of a Small Flux Rope in the Chromosphere Observed by NST, IRIS, and SDO, 2015, P. Kumar, V. Yurchyshyn, H. Wang, & K.S. Cho, Astrophys. J., 809/1, article.id 83
11. Dynamics in Sunspot Umbra as Seen in New Solar Telescope and Interface Region Imaging Spectrograph Data, 2015, Yurchyshyn, V., Abramenko, V., & Kilcik, A., Astrophys. J., 798, article.id 136

B. Proposed Research

B.1 Current GST Instrumentation

The proposed work will enable us, and community users of GST data, to reap the benefits of AFOSR investments made into the GST and its instrumentation. In fact, the first major funding for the GST came from AFSOR-DURIP support. Much of the GST instrumental sketched below benefited from AFOSR support and will be used in the work proposed here.

Goode Solar Telescope (GST) with Adaptive Optics (AO). The GST optical systems and instrumentations (Goode et al., 2010; Cao et al., 2010; Goode et al., 2012) offer a significant improvement in ground-based, high angular resolution and polarimetric capabilities and were built with support from the AFOSR and NSF: while the NSF funding was the primarily supporting building of the GST, the AFOSR was primarily providing funds for the post-focus instrumentation.

We have developed, in collaboration with NSO, an AO system based on a commercially available, 357 actuator DM (AO-308, 308 subapertures on the lenslet array), and we realistically achieved a Strehl ratio of 0.3 in the detector plane in the visible (0.5 μm) under nominal BBSO seeing conditions. This system is subsequently upgraded by CAO and GLAO systems and *Clear* will follow later. The Strehl, generally used to quantify the performance of an AO system, is the ratio of the maximum intensity in the AO corrected image in the detector plane to that from a theoretical, perfect imaging system operating at the diffraction limit. Our 357 actuator DMs from Xinetics have a special faceplate made of silicon instead of ULE (ultra-low expansion glass) because silicon has about 100 times the thermal conductivity of ULE to conduct away the heat on the DM from the Sun. We have implemented a more complex digital signal processing (DSP) system and a faster wavefront sensing camera from CAO with Quasar having provided the camera to DSP and DM to DSP interfaces.

Near InfraRed Imaging Spectro-polarimeter (NIRIS, Cao et al., 2011, 2012) is a a dual Fabry-Pérot etalon system allowing us to fine tune to any wavelength between 1.0 and 1.7 μm. The hardware for NIRIS and its forerunner IRIM was acquired under AFOSR-DURIP support. NIRIS's FPI etalons provide a large, 85″, field of view and great throughput resulting in a faster scan cadence of 1 sec for spectroscopic and 10 sec for full Stokes polarimetric measurements. The dual-beam optical design will image two simultaneous polarization states onto a 2024x2048 HgCdTe closed-cycle He cooled IR array. The primary lines of interests for NIRIS are the Fe I 15650Å doublet, which is the most Zeeman sensitive probe of the magnetic field in the deepest photosphere and the He I 10830Å multiplet that is the best currently available for diagnostics of upper chromospheric magnetic fields.

Visible Image Spectrometer (VIS) utilizes an FPI etalon with a bandpass of 0.1Å and the possibility to shift the bandpass by 2Å around the Hα line center. The pixel scale is set to 0″.027 and the FOV is 69″ by 58″. A full line scan with a 0.2Å step (11 positions) can be performed with cadence of about 5 s. Images at one arbitrary position can be taken with a much higher cadence. VIS is currently being upgraded to a dual FPI, like NIRIS, to cover from 550 nm to 860 nm. The upgraded VIS should be online, before the start of the work proposed herein.

Fast Imaging Solar Spectrograph (FISS Chae et al., 2013) is a field-scanning slit spectrograph with high spectral resolution (1.4×10^5) and scanning speed (10 s) able to sufficiently cover a FOV of $40'' \times 60''$. Two different major spectral lines such as Hα, Ca II H and K, and Ca II 854.2 nm can be recorded simultaneously using two CCD cameras, which allows to distinguish between the thermal component and the non-thermal turbulence, so that a precise determination of temperature is possible.

KISIP Software for Speckle Reconstruction. The Kiepenheuer-Institut für Sonnenphysik's software package for speckle interferometry of adaptive optics corrected solar data (KISIP) is a post AO reconstruction algorithm

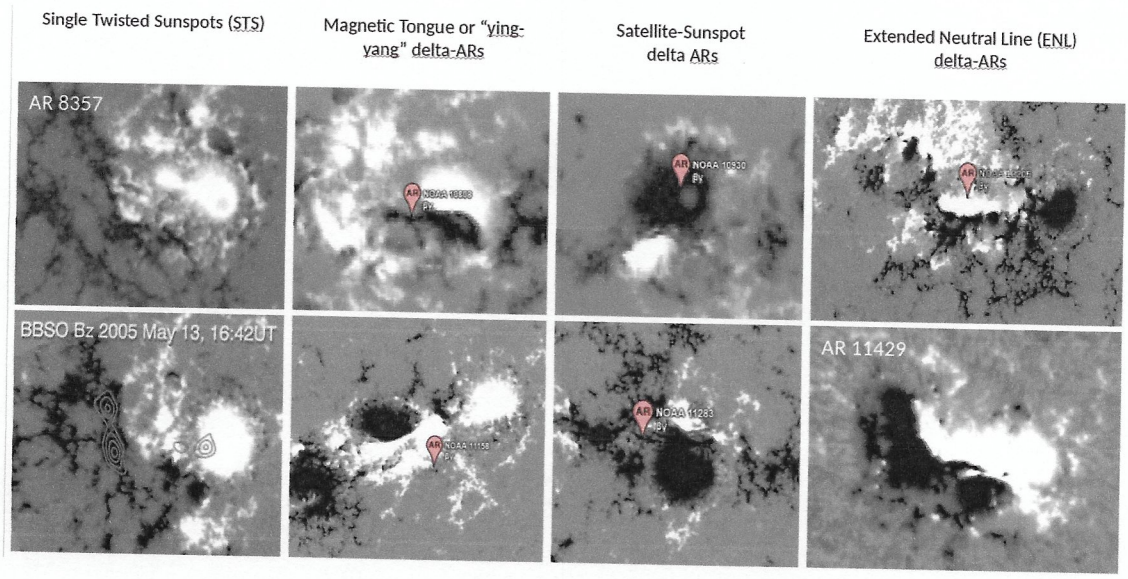

Figure 4: *Four main AR types that are capable of producing powerful eruptions associated with fast and geoeffective CMEs.*

allowing to achieve the diffraction limit (Wöger & von der Lühe, 2007). The code has been written in C programming language and optimized for parallel processing on BBSO computers.
MultiConjugate Adaptive Optics (MCAO) system has enjoyed a successful first light in which the MCAO effectively tripled the size of the isoplanatic patch over an ordinary AO with a single DM. The expansion of the diffraction limited FOV will be sufficient to cover entire active regions (which include, for instance, flares that might occur anytime and anywhere in an active region) enabling spectroscopic and polarimetric observations with a sub-second cadence instead of the 10 s time cadence available now after post-facto image reconstruction. Therefore, the MCAO system will eliminate a major limitation of conventional AO systems, the insufficiently large isoplanatic patch, and, thus provide the tool to effectively study, with the requisite high temporal cadence and with the GST's unprecedented spatial resolution, fundamental scientific questions like the onset and evolution of flares, flare triggering mechanisms, magnetic reconnection events and many other dynamic solar phenomena, which would be best performed with diffraction limited observations over an extended FOV at sub-second temporal cadence.

We plan to use MCAO in the studies of dynamical active regions and quiescent filaments to probe the origins of space weather with precision never seen before. Such observations will be the most significant as well as being a straightforward use of MCAO and we plan for them in the second year of the proposed study. Most of the GST instruments described above will be used in the work proposed here.

B.2 Understanding Sources of Coronal Mass Ejections

Coronal Mass Ejections (CMEs) have long been identified as a prime cause of large, non-recurrent geomagnetic storms (e.g., Burlaga et al., 1981; Tsurutani et al., 1988; Gosling et al., 1990; Zhang et al., 2007). Solar plasma and magnetic fields ejected into the heliosphere as a result of an eruption are further propelled into interplanetary space to become an interplanetary CMEs where it may encounter the Earth and produce large southward excursions of the interplanetary magnetic field. ICMEs often exhibit a flux rope structure, meaning that they harbor a large-scale, coherent loop-like structure with large amount of twist. Many studies have illustrated that the sense of magnetic twist and the direction of the fields in ICMEs matches those of the source region, thus opening a pathway for predicting the likelihood of geomagnetic storms (e.g., ?Yurchyshyn et al., 2005; Gopalswamy et al., 2007, , and references therein) and the CME speed may be related to the magnitude of the associated storm (e.g., Yurchyshyn et al., 2004; Srivastava & Venkatakrishnan, 2004; Yurchyshyn et al., 2005).

It is therefore important for forecasters to understand details of erupting magnetic configurations to be able to make a short term flare prediction. The community's flare forecast effort was mainly focused on the possibility of predicting a flare by analyzing magnetic field measurements (e.g., Georgoulis, 2008; Falconer et al., 2014; Tiwari et al., 2015; Barnes et al., 2016). This effort is best summarized by Barnes et al. (2016) who concluded during the "all clear" forecast workshop that "no one method clearly outperformed all others". When prediction of M-class flares and above was tested a "set of methods tends toward a weakly positive skill score ... with no participating method proving substantially better than climatological forecasts". All tested methods were based on analysis of instantaneous AR parameters without considering the long term evolution of an AR, flaring history, or the type of magnetic configuration involved.

Here we propose a new approach that will improve our understanding of flare productive ARs and may lead to new flare forecast techniques. It is based on extensive studies of a certain type of eruptive ARs. Using a list of CMEs and their solar sources compiled by Zhang et al. (2007), we carefully inspected the active regions (ARs) that produced very fast (>1200km/s) CMEs in solar cycle 23. Out of total 81 analyzed events, 52 event occurred in "δ"-configurations (Fig. 4), 15 in configurations with a dominating single twisted sunspot (STS, Fig. 4, left column) and 14 originated from magnetic complexes. We reviewed the ARs that produced strongest flares in cycle 24. Better quality HMI data allowed us to further separate "δ"-configurations into three subgroups, which we describe as: i) "magnetic tongue" (Poisson et al., 2016) or "yin-yang" ARs (Fig. 4, 2nd column); ii) satellite-sunspots (Fig. 4, 3rd column, also see the 13 Dec 2006 Hinode sunspot); and iii) ARs with an extended neutral line (ENL, 4th column). The "yin-yang" ARs are highly sheared and twisted structures and are very similar to the "satellite-sunspot" ARs with the only distinction that the opposite polarity sunspot in the satellite configuration is significantly smaller than the main sunspot to which it is connected. In turn, the ENL types can be viewed as a chain of satellite or "yin-yang" configurations aligned along the AR axis.

We will do the following: We will update the list of fast eruptions during cycles 23 and 24. Between Sept 2005 and Dec 2016 There were 110 CMEs with speeds above 1000 km/s. We will identify the source of each of those fast CMEs and determine the type of magnetic configuration involved in an eruption. Second, we will create a profile for each of these typical configurations. This means we will quantify and compare evolution of ARs within one group aiming at answering the following main science questions: *Do ARs of the same type evolve in a similar way? Can we create a profile for, say, an "average" STS AR and use it for predicting the location and time of future eruptions from the same type of configurations?* For example, the two STS ARs in Fig.4 (left panels) appeared at the east limb as developing 2-3 days old ARs. They all produced morphologically similar flares and eruptions nearly 7 days later when they reached the central meridian (e.g., Yurchyshyn et al., 2000, 2006). *Is this time lag between the onset of emergence and the major eruption a coincidence, or does it reflect some inherent properties that govern development of this particular type of ARs?* On the other hand, strong "δ"-configurations behave differently: NOAA ARs 10488 and 21094 (to name few) observed in Oct 2003 and Sept 2017 produced their most powerful flares after only 3 days of development. NOAA AR 12371 erupted on the 4th day (22 June 2015) after the "δ"-sunspot emergence onset. Clearly, different magnetic types evolve along different tracks and we must develop an "individual" approach to each of the types to succeed in understanding, modeling and predicting their behavior.

We will start from the STS type since it is the simplest of all types and has the most pronounced configuration. Creating a profile of a typical STS AR will include studying temporal properties of magnetic and flow fields and flaring activity as well as identifying a common evolutionary pattern. Our earlier studies of STS sunspots (Yurchyshyn, 1997; Yurchyshyn et al., 2006, 2000; Yurchyshyn & Wang, 2001) indicate that there are strong flows converging toward the core of the AR where eruptions had initiated. These flows along with the relatively long quiet period before the eruption may suggest the type of energy build up mechanism that may operate in such ARs. An eruption on 12 May 1997 in NOAA AR 8038 that is of the STS type was designated as an "SHINE event" and it was extensively studied by various groups (e.g., Baker et al., 1998; Thompson et al., 1998; Gopalswamy et al., 2017). Certainly we will use these finding as well and incorporate them into the STS AR profile. The approach and techniques developed and tested while working on the STS types will be later used to create "average" profiles for the "δ-configurations.

Next, we will perform non-linear force free field (NLFFF) modeling of an AR of one type in order to understand the details of their magnetic configuration and their evolution. To do that we will exploit the

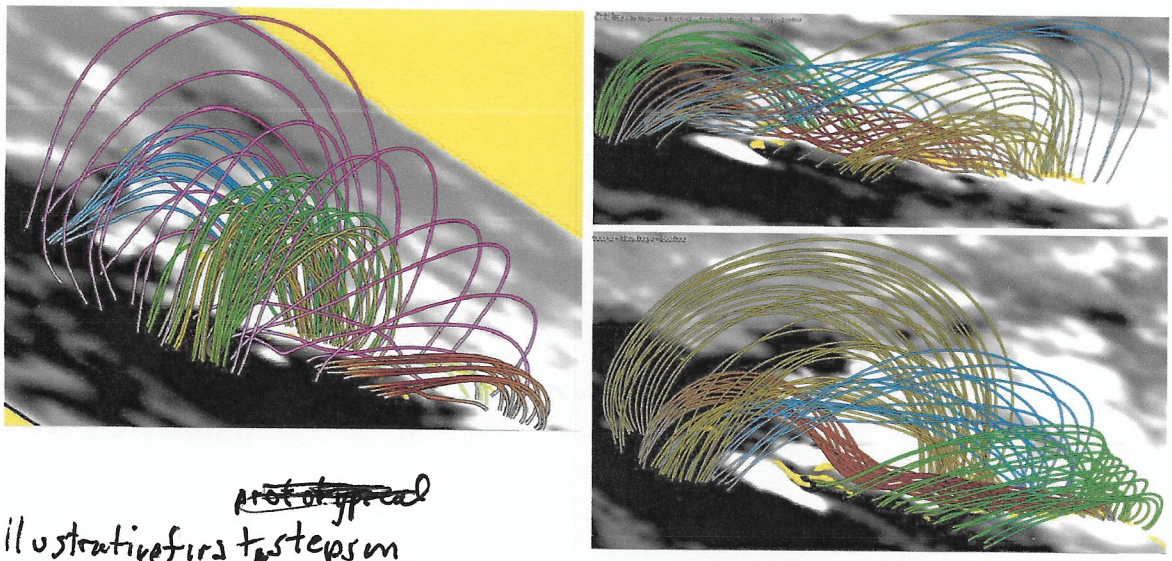

Figure 5: *Snapshots of NLFFF lines calculated for AR 12192 on 2014 Oct 22 (left), 24(top right), and 25 (bottom right). The red lines in the right panel outline a flux rope and the multicolored lines represent various parts of the overlying fields. The Oct 22 model does not show any presence of organized helical fields (left panel). However, during two days of evolution the fields continued to be stressed and eventually a flux rope was formed according to this NLFFF simulations.*

NLFFF method developed and tested by (e.g., Jiang & Feng, 2013; Jiang et al., 2016, and references therein). In fact, this modeling effort has already begun and we developed a technique that allows us to detect and visualize the existence of a simulated flux rope (FR) in an NLFFF configuration. In Fig 5 we show three snapshots of NLFFF lines calculated for NOAA AR 12192 on 22, 24, and 25 Oct 2014. The red lines in the two rightmost panels represent a FR, while the multicolored lines represent various parts of overlying fields. The Oct 22 model does not show any solid evidence of organized helical fields yet (left panel). However, during two days of evolution magnetic structure continued to be stressed and eventually a FR was formed according to this NLFFF simulations. Jiang et al. (2016) performed data driven MHD simulation of this AR and noted formation of a strong current sheet above the neutral line. We would like to understand the details of this process. We will do it in two different ways. On one hand we will model one AR of each type (STS, satellite-sunspot and extended NL types) using a HMI SHARP-CEA set taken every 6 hours. The simulation and data analysis tools are on-hand on BBSO computers and can be easily used to expand this research. We will review and use relevant simulations and observations already published in order to create a comprehensive road-map of evolution of a certain AR type.

We are aware of problems that accompany NLFFF modeling. DeRosa et al. (2015) concluded that NLFFF solutions do depend quantitatively on the spatial resolution of the input data, and to obtain more self-consistent results more highly resolved boundary data is needed. We will use HMI data, which is at this moment the best quality data set routinely available for modeling. These authors also recommend verifying agreement between the modeled field lines and corresponding coronal loop images before any NLFFF model is used in a scientific setting. This has been done for this numerical tool on many occasions. We will test our simulation results at every 6-hours step to ensure that we are on the right track. We also note the simulations will be used to understand how coronal magnetic fields react to changing photospheric conditions, therefore some deviations from the real configuration will not be very critical as long as we consistently use the same numerical tools and input data.

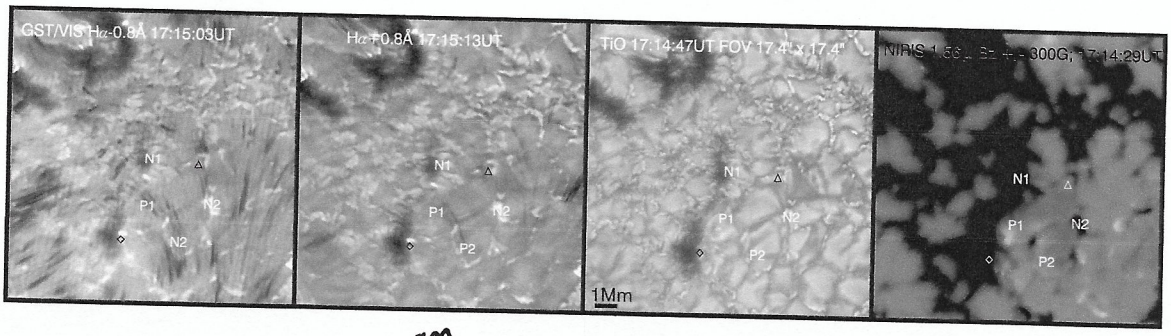

Figure 6: *GST images of an area where an AIA loop was rooted. From left to right: Hα-0.8 Å, Hα+0.8 Å, TiO images and NIRIS Bz map. Letters and symbols mark several key magnetic elements. The AIA 171 Å loop footpoint was located between N1, N2, P2, and P1.*

B.3 Small-Scale Magnetic Dynamics, as Possible Photospheric Sources of Coronal Heating and Dense UV Loops

Complete understanding of coupling between the magnetically-dominated corona and the pressure dominated photosphere has been an elusive goal of many past investigations. High-resolution GST images of coronal loops at low temperatures (e.g., Ji et al., 2012) provide a new and unrivaled means for exploring this link along with G-band (4305 Å), TIO band (7057 Å) and NIRIS data that reveal magnetic flux in dark inter-granular lanes at footpoints of these loops. Thus, Ji et al. (2012) was able to trace coronal 10830 Å loops as thin as 100 km down to their roots in a dynamic intergranular lanes. Jing et al. (2016) identified co-spatial and co-temporal IRIS UV and GST Hα brightenings and concluded that GST captured finer components of an M-class flare in deeper, cooler and denser chromosphere.

To explore physical origin of ultra-fine loops (as well as other fine-scale associated processes), GST magnetic field data should be combined with UV observations (AIA, IRIS) and MHD modeling to measure the dynamics of loops footpoints and Stokes profiles in various magneto-convection conditions, magnetic field strengths and topologies. Solving inverse problem for observed Stokes profiles will allow us to estimate physical parameters, such as plasma temperature, density, velocity and the magnetic fields, which can further be compared with numerical simulations.

GST/NIRIS instrumentation now offers us for the first time a new possibility to investigate the role that flux emergence and cancellation may play in driving mass and energy flows within coronal loops and as well as other recurring and intermittent flows. Brooks et al. (2008) used Hinode data to report that coronal loops and transient brightenings are rooted in areas with dynamic magnetic fields. The problem is that many fine loops were found to be rooted in *unipolar* fields as seen in Hinode data, which led authors to suggest that the heating in transient brightnenings may be fundamentally different than that in coronal loops.

While there are numerous studies of physical conditions in coronal loops (see review by Reale, 2014), studies of the underlying magnetic fields are lacking and the role of the magnetic field is viewed through the stereotype that plage fields are unipolar and unmixed, the view which is now being challenged by high-resolution observations and simulations. Thus, simulations by Rempel (2014) revealed complex and intermittent magnetic and flow patterns in intergranular lanes suggesting that there is magnetic complexity currently not detectable by most instruments. GST/NIRIS data showed small-scale mixed polarity magnetic fields surrounding a magnetic cluster (Yurchyshyn et al., 2013) and magnetic cancellation was omnipresent at this location. Abramenko et al. (2009, 2013) analyzed Hinode and GST data and reported that on spatial scales below 2 Mm magnetic fields are of mixed polarity and complex, which favors burst-like energy release.

Here we show one example that encourages us to pursue this topic (Şahin et al. 2018, in preparation). The field of view in Fig. 6 encloses a footpoint of a faint AIA 171 Å loop with a small UV brightening at its end located between N1, N2, P2 and P1. GST/TiO data at that location showed granular evolution (fast flows, elongated granules) consistent with emergence of small-scale fields. Small-scale point-like brightenings can also be seen in off-band VIS Hα images (below N1 and at N2, diamond). Most importantly, a co-temporal NIRIS Bz

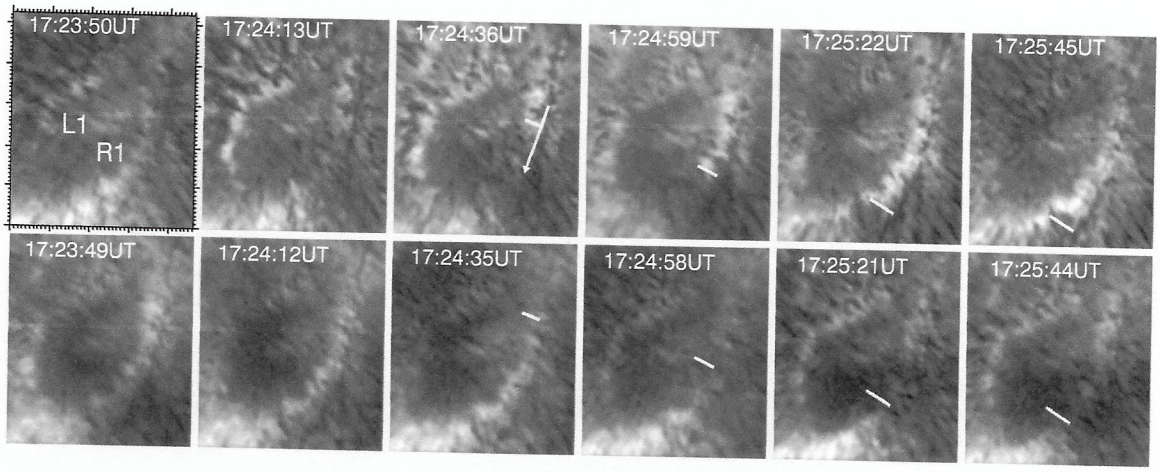

Figure 7: *Dynamics of UFs as seen in GST Hα+0.4Å (top) and Hα-0.4Å (bottom) images. L1 and R1 mark locations of two bright UF lanes. The short line segments mark the edge of an expanding UF lane, while the arrow shows the direction of expansion. The dashed curves indicate the position of LBs. The large tick marks in the leftmost top panel indicate 1 Mm intervals.*

map shows several elements of parasitic polarity embedded in the negative (black) plage field (P1 and below) and P2 and N2 elements are seen to form an emerging bipole. We argue that these emerging fields interacted with large-scale fields rooted at the N1 cluster and due to interchange reconnection the N1 footpoint has to shift to N2, which was reflected in the evolution and displacement of the UV loop. The spatial scale of these fields is of order of 0.5 Mm or less, which is quite difficult to measure and it can only be done under very good and stable seeing conditions using high power instrumentation.

We will use our existing extensive GST archive to identify temporal and spatial windows of high quality GST data. We will search SDO/AIA 171 Å images for evolving isolated loops with at least one footpoint within these windows. We select the 171 Å channel because it allows us to easily spot a single loops and reliably identify its footpoints. We will produce *x-t* plots from curved cuts along the loop axis to properly document the loop evolution. Using AIA images from other temperature ranges, we will measure the loop temperature, density and EM at the peak of evolution. We will identify location of the loop footpoints in NIRIS photospheric magnetograms and BFI-TiO images and will determine evolution of the associated magnetic background. The footpoint study will also be aided by GST off-band Hα data to accurately pinpoint the process responsible for loop activation. We will carefully compare magnetic dynamics with the evolution of UV loops to ensure that these two phenomena are reliably related. These studies will be performed in both active regions and quiet Sun areas. We will address the following science questions. *How often active UV loops are associated with magnetic flux emergence and cancellation at their footpoints? What are parameters of the emerging/canceling fields? How high in the corona do they penetrate before loop activation starts (i.e., time lag between the first signs of emergence and coronal activity)? What kind of loop activity is typically observed in association with flux emergence and cancellation? Are there chromospheric (GST Hα, Ca II K) and/or transition region (IRIS) signatures of this process?*

B.4 Sunspot Umbral Flashes and Oscillations in GST and IRIS Data

Yurchyshyn et al. (2015) observed two types of umbral flashes (UFs): i) weak and diffuse UFs, which are observed over the darkest parts of the umbra with strongest fields, and ii) bright UF lanes running along LBs and clusters of umbral dots (UDs, Figure 7). While the diffuse UFs tend to appear and fade at the same location, the lane UFs show horizontal motions, i.e., a UF lane expands along a LB. They also tend to be brighter and last longer.

The tendency for the lane UFs to be associated with strong magneto-convection umbral features is intriguing and potentially beneficial for solving the mystery of coronal heating. We realize that without MHD simulations

of sunspots, we will not be able to provide a compelling answer to the question why the lane UFs appear at LBs. As far as we know, realistic MHD simulations of the atmosphere above sunspots are not yet available, therefore studies of high-resolution data are currently the only source of new knowledge on sunspots. However, Hollweg et al. (1982) found that when Alfven speed, v_A, decreases with height, then shocks form more effectively. Such conditions are met in sunspots in rapidly expanding vertical flux tubes that neighbour LBs and UD clusters, which are considered to be field-free structures to a certain extent. The fact that LBs and UDs are also co-spatial with foot-points of dense coronal loops suggests lane UFs and LBs may be an important contributor to the heating process and need to be understood.

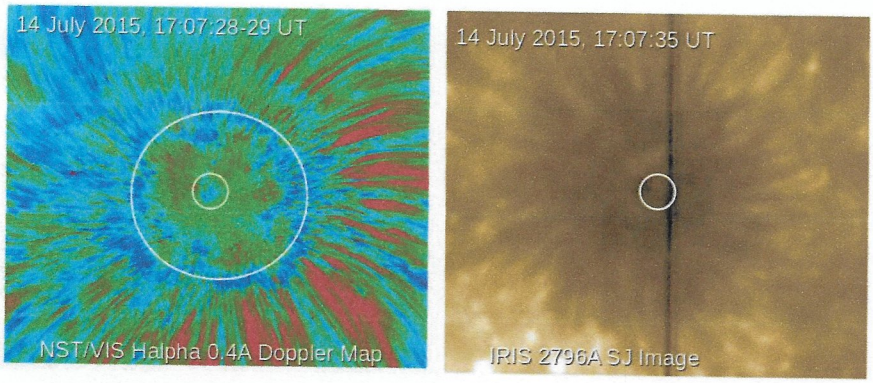

Figure 8: *Left: NST VIS Hα-0.4 Å Doppler map with blue pixels indicating upwelling in the running waves and the green areas indicate plasma falling down. Right: Co-temporal IRIS 2796 Å slit-jaw image. The red colors are strong jet-like downflows that abruptly end at the outer edge of the penumbra. The large circle highlights the circular shape of the running wave (blue). The small circle encloses a small and growing blue-shifted patch, which will become another running waves.*

In Fig. 8 we show data from one of our BBSO-IRIS campaigns designed to measure propagation of umbral and penumbral waves using both slit-jaw images and spectroscopy. The left image is an H-alpha 0.4 Å Doppler map and the large circle highlights a nearly circular penumbral wave (blue, upwelling) that has evenly spread from the center of the sunspot. The small circle in the middle of the umbra encloses a growing blue patch, which is the onset of another umbral wave. The co-temporal IRIS image shows bright 2796 Å UF enclosing the small circle on the left and co-spatial with the H-alpha down-welling phase of the expanding umbral wave (green). These data collected for a single, simple, and round sunspot suggest that here we deal with a single and compact sub-photospheric driver of oscillations. According to Felipe et al. (2010), simulations when a fast (acoustic) wave moves horizontally across the umbra, up and away from a compact sub-photospheric source located near the axis of a sunspot, it is partially converted into a slow mode wave when it reaches the layer where the Alfven and sound speeds are equal. The slow mode waves then steepen into shocks, thus creating a pattern of shocks and UFs propagating away from the sunspot center. This behavior, inferred from simulations, is very similar to the dynamics of UFs observed here.

However, sunspots with a more complex structure (e.g., two or more umbral cores, LBs, etc) show more a complicated pattern of waves propagation. Possibly it is because we are dealing with several compact sources of oscillations. We are now studying the GST and IRIS data for the above case in details (Kilçik et al. 2018, in preparation) in order to understand this simple case of wave propagation and then transfer the knowledge to other more complicated cases. Moreover, sunspot running waves are also associated with umbral spikes (Yurchyshyn et al., 2014), which are oscillating jet-like 0″.1 features. We will search for another source of oscillations in case the pattern is disrupted. Although the wave in Figure 8 *appears* circular, it is also "broken" or weak in several locations. We will address the following science questions: *Is our inference about the two types of UFs valid for other sunspots? Are there preferred locations for appearance of diffuse UFs? What determined the wave propagation rate? Are there certain magnetic structures that promote or hinder the wave propagation? What is the role of LBs in wave generation? Are these enhanced lane UFs always associated with LBs? Are sunspot oscillations driven by one or several sub-photospheric drivers? What defines the location and the number of these drivers? Do different UFs have distinct spectral signatures and physical parameters?*

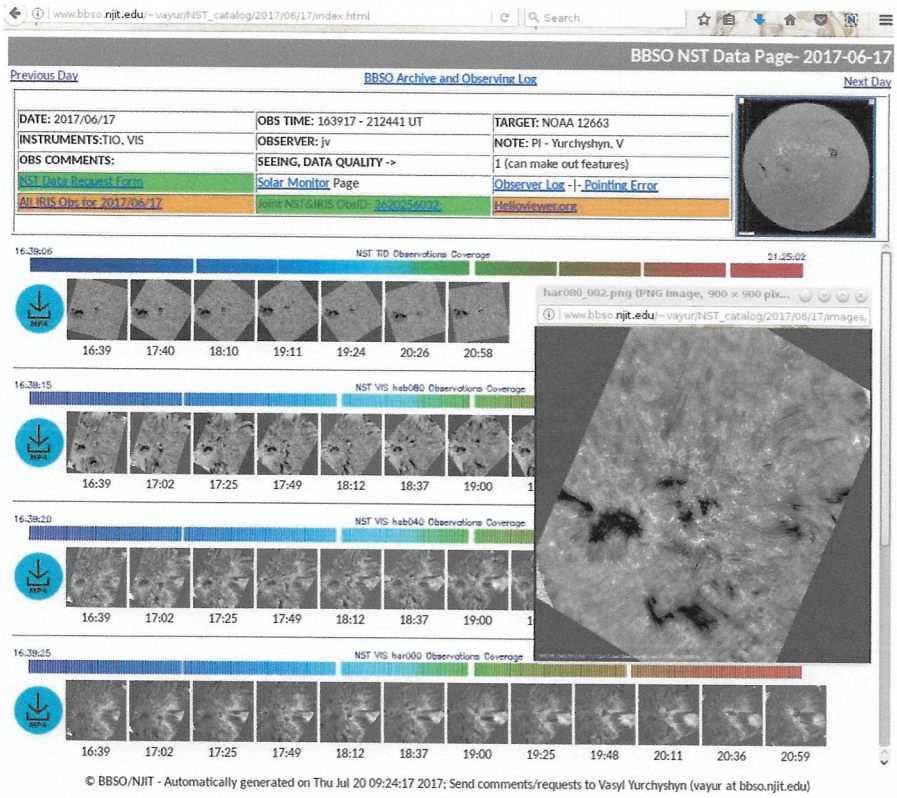

Figure 9: *Redesigned NST catalog. Typical data frontpage shown for 17 June 2017. Small squares plotted over the BBSO full disk Hα image indicate where GST observations were taken. The page header displays information about the data, provides direct links to relevant IRIS, SolarMonitor.org and Helioviewer.org web pages as well as to Data Request Form. Ten quick look images are available for each wavelength (see insert), as well as quick look movies.*

Spectral data necessary to address this last question are currently available from a narrow band imager (VIS) that is capable of scanning the Hα spectral line and double spectrograph (FISS) produces spectral data using in the Hα and Ca II 8542 Å spectral lines.

Our experience shows that to address these questions we need high-cadence data with a high-resolution over a wide FOV, so that the entire sunspot can be imaged with necessary precision. While the narrow band VIS images can be speckle reconstructed to improve image quality over a FOV larger than the AO isoplanatic patch, FISS data can not be reconstructed in the same way. The new MCAO system will mitigate this problem by achieving diffraction limited resolution over a large (≈ 50″) FOV so that quality FISS spectra and NIRIS magnetic field measurements covering the entire sunspot can be obtained.

C. Providing Data to the Community

On a typical observing day, the NST collects about 0.5 TB of raw, AO corrected data per channel (2-3 channels/day). Acquired NST data from each channel are post-processed to about 5 GB (dark current and flat field corrections, as well as speckle reconstruction for photometric data and calibration for polarimetric data) and placed in the BBSO archive system. A quick look web page is then generated (Figure 9) aimed to provide sufficient information to make it easy for users to search for NST data. Users can then use an automatic request form, which will enable them to download data over Internet.

We continue to develop this data distribution system. Now quick look, low spatial resolution (0″.1/pixel) movies are available at *www.bbso.njit.edu/~vayur/NST_catalog/* for each of the wavelength observed. The requested data are put on our ftp server for users to download (*ftp://ftp.bbso.njit.edu/pub/nst_data_requests/*). Our future improvements will be focused on extracting and providing descriptive metadata for existing and new NST data, so this information can be easily integrated into community data centers, such as Virtual Solar Observatory and Heliophysics Events Knowledgebase. Another direction that we will be working on is to create and make public a set of software tools necessary for data preparation, such as de-rotation, alignment, manipulation of spectral data, etc, which will facilitate access to NST data for outside users.

D. Education and Research Training

We currently have one Ph.D. student permanently residing at the observatory. 75% of our more than twenty Ph.D. graduates since 2000 now hold technical positions in the U.S., including eight working in solar physics research. Twelve former students/postdocs from our group have moved on to faculty/national center positions. This includes five in the U.S. The very best NJIT students are attracted to the BBSO programs. The typical student designs and builds the instruments used to make his/her Ph.D. measurements in BBSO. These students can also utilize the laboratories and ~~our small observatory~~ on campus to test the instruments for use at BBSO. We seek nine months of funding per year for research professor Vasyl Yurchyshyn who is a co-PI on this proposal. He is primarily responsible for the delivery of the science proposed here. He will marginally involved in the instrumentation and lead in data reduction and interpretation of the data required to perform the tasks enumerated above. As well, he will prepare and implement the NST data pipeline and ensure the quality of all data place online from BBSO. He prepared the existing pipeline that he will upgrade.

E. Personnel and Management

PHIL: IS WENDA PART OF THIS PROPOSAL?

The role and tasks of team members are the following. PI, P. Goode will monitor the progress of the project and ensure a proper connection between instrumentation and scientific return. Co-PI W. Cao was the key scientist in building, testing and deploying the NIRIS and he will be responsible for focal plane instrumentation. Co-PI V. Yurchyshyn is the key scientist in residence at BBSO. The current grant has supported Vasyl Yurchyshyn.

F. SECTION FROM PREV PROPOSAL, HAS NOT BEEN UPDATED YET: Budget Justification

This is a three year project with a total budget of $420 K. The proposed budget will cover about 75% of Dr. Yurchyshyn's salary, which is $85,000 for the first year and inflates at 3.5% per annum, and the fringe benefit rate is 48.3% on the salary. The budget includes $4,000 per year to cover the cost of two trips per year to domestic professional meetings for Dr. Yurchyshyn. The budget also includes annual costs of $2,000 for publication charges. The AF OH rate is 35% and is applied against all the aforementioned costs. Performing the proposed work would be a unique opportunity for Dr. Yurchyshyn, as well as Goode and Cao.